

Mechanical characterization of plasma sprayed ceramic coatings on metal substrates by contact testing

Antonia Pajares^{a,1}, Lanhua Wei^{a,2}, Brian R. Lawn^a, Nitin P. Padture^b,
Christopher C. Berndt^c

^aMaterials Science and Engineering Laboratory, National Institute of Standards and Technology, Gaithersburg, MD 20899, USA

^bDepartment of Metallurgy and Institute of Materials Science, University of Connecticut, Storrs, CT 06269, USA

^cDepartment of Materials Science and Engineering, State University of New York at Stony Brook, Stony Brook, NY 11794, USA

Received 1 August 1995; in revised form 12 October 1995

Abstract

Hertzian indentation testing is used to generate contact damage in plasma sprayed ceramic coatings on metal substrates. Two basic ceramic/metal coating/substrate systems are examined: alumina on steel and zirconia on superalloy. Macroscopic mechanical responses are measured via indentation stress–strain curves, which quantify the relative role of the coating and substrate in the net deformation and facilitate evaluations of elastic moduli and yield stresses. Micromechanical damage processes within the coating and substrate subsurface layers are studied using a “bonded-interface” specimen. Degradation occurs primarily by delamination and other cracking at the coating/substrate interface or in the coating, but plastic deformation of the metal substrate contributes importantly to the crack driving force.

Keywords: Coatings; Contact damage; Delamination; Fracture; Indentation stress–strain curve; Plasticity

1. Introduction

Ceramic coatings on metal substrates are of practical importance, notably for thermal and wear resistance. Those coatings produced by thermal spray methods tend to have highly defective laminar microstructures, with weak interfaces and voids between solidified splats [1–4]. It is this discretely weak interface structure that primarily characterizes the properties of the coatings. Whereas defects can degrade the strength of the coating structure, they can also accommodate mismatch strains and improve thermal insulation. The coatings are subject to failure from deformation and fracture under thermal, mechanical, or internal stresses, and the deformation properties of the substrate can contribute to the failure mode [5,6].

The mechanisms of damage evolution in plasma sprayed coatings in different stress states, especially

cyclic stresses, have not been extensively studied. Test procedures are most often engineering-oriented, geared toward lifetime evaluations under service (or simulated service) conditions [4], and are not always well suited to investigating fundamental material properties. Much attention has been given to delamination, particularly between the coating and substrate. The presence of a metal-based bond coat can help alleviate this delamination. There is a need to understand how competing deformation and fracture modes can be influenced by the defect microstructure, and can lead to final coating failure.

Here we demonstrate the use of a Hertzian contact method to investigate these deformation and fracture modes. This method has been used previously in studies on bulk ceramics with heterogeneous microstructures, i.e. weak internal boundaries, large and elongate grains, and high internal stresses [7–12]. Whereas the introduction of heterogeneity confers toughness (at least in the long-crack domain), by grain bridging [13,14], it also induces a fundamental transition in the Hertzian contact response, from ideal brittle to quasi-plastic [15]. The quasi-plasticity is attributed to accumulation of

¹ Guest Scientist, Departamento de Fisica, Universidad de Extremadura, 06071-Badajoz, Spain.

² Guest Scientist, on leave from Department of Physics and Astronomy, Wayne State University, MI 48201, USA.

discrete damage at the weak points in the subsurface zone. More recently, the contact procedure has been extended to some simple model layer structures with a hard, homogeneous (brittle) layer on an underlying tough, heterogeneous (quasi-plastic) layer [16,17]. Energy absorption in the deformable substrate can help contain coating failure.

In this study the Hertzian test is used to examine two model plasma sprayed ceramic/coating systems: (i) alumina/steel, without bond coat; and (ii) zirconia/superalloy, with bond coat. These two material systems usefully demonstrate elastic–plastic mismatch effects: in the first, the coating is harder than the substrate; in the second, the reverse is true. Indentation stress–strain curves reflect competing brittle–plastic damage modes, and quantify the increasingly important role of the substrate with expanding contact radius. Estimates of elastic modulus and yield stress are obtainable from these data. “Bonded-interface” specimens [8,9] provide section views of fracture in the ceramic coatings and plasticity in the metal substrates, and delamination between the layers. These damage patterns are considered in terms of the contact fields beneath the spherical indenter, with special attention to interlayer mismatch.

2. Experimental

2.1. Materials

Two plasma-spray material systems were chosen as models for study, partly for their ease in preparation and partly for their relevance to thermal barrier and wear resistant coatings. In each system, substrates > 3 mm thick were blasted with alumina grit to provide an appropriate surface topography for enhanced adhesion, and subsequent plasma spraying of the coating was carried out in air. Selected specimens were sectioned, given a final polish with $1 \mu\text{m}$ diamond paste, and gold-coated for microscopic characterization in Nomarski illumination. Porosity evaluations were made from these sections by digital analysis of computer-scanned images.

2.1.1. Alumina/steel

Alumina coatings were sprayed to a thickness $d \approx 500 \pm 100 \mu\text{m}$ (specimen-to-specimen variations, four specimens) directly onto soft steel substrates, without bond coats. In these specimens, the plasma torch made four passes in approximately equal intervals (the interruptions in the spraying schedule imposed simply to prevent the substrate from overheating). The section in Fig. 1(a) reveals the interruptions as remnant interfaces within the coating. From the digital analysis, the porosity of the alumina coatings is $\approx 8\%$ (Table 1).

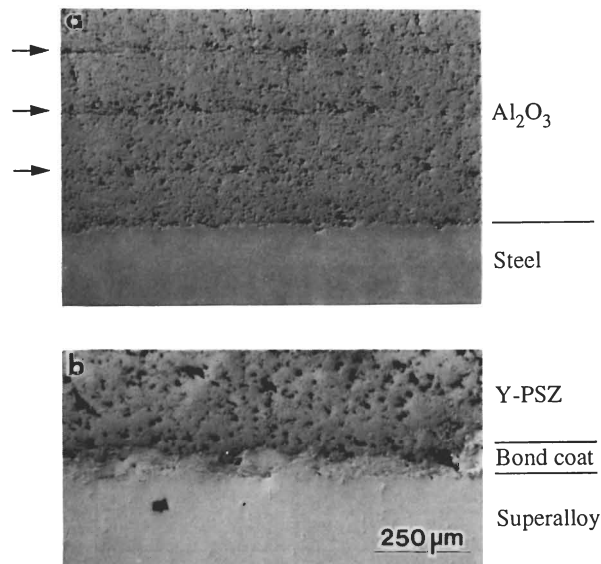


Fig. 1. Optical micrographs, showing sections of (a) alumina/steel, (b) zirconia/bond-coat/superalloy. Note porosity of both coatings, and layers (arrows) in alumina. Nomarski illumination. (Magnification same in both micrographs.)

2.1.2. Zirconia/bond-coat/superalloy

Coatings of 8 wt.%-yttria-partially-stabilized zirconia were sprayed to a thickness $d \approx 300 \pm 30 \mu\text{m}$ (four specimens) onto relatively hard nickel-based superalloy substrates, but this time with $\approx 50 \pm 20 \mu\text{m}$ Ni–Cr–Al–Y alloy bond coats. Fig. 1(b) is a section view. The porosity of the zirconia coatings is $\approx 12\%$ (Table 1).

Some specimens were also prepared from bulk free-standing coatings and substrates, each again > 3 mm thick, to provide reference conditions for the ensuing indentation data.

2.2. Indentation tests

Hertzian contact tests were carried out as depicted in Fig. 2, using tungsten carbide spheres of radius $r = 1.98\text{--}12.7$ mm. Peak loads up to $P = 5000$ N were delivered by a screw-driven Instron testing machine (Model 1122, Instron Corp., Canton, MA). Prospective test surfaces were surface-polished with $1 \mu\text{m}$ diamond paste. All experiments were conducted in air.

Table 1

Porosity, Young's modulus E and hardness H for bulk coating and substrate materials. Modulus derived from slope of stress–strain curves (Fig. 3 and Fig. 4). Hardness measured directly from Vickers indentation tests

	Porosity (vol.fract.)	E (GPa)	H (GPa)
Al_2O_3	0.08	80 ± 4	5.4 ± 0.6
Steel	0	180 ± 36	1.2 ± 0.1
ZrO_2	0.12	30 ± 6	1.8 ± 0.3
Superalloy	0	230 ± 12	4.2 ± 0.1

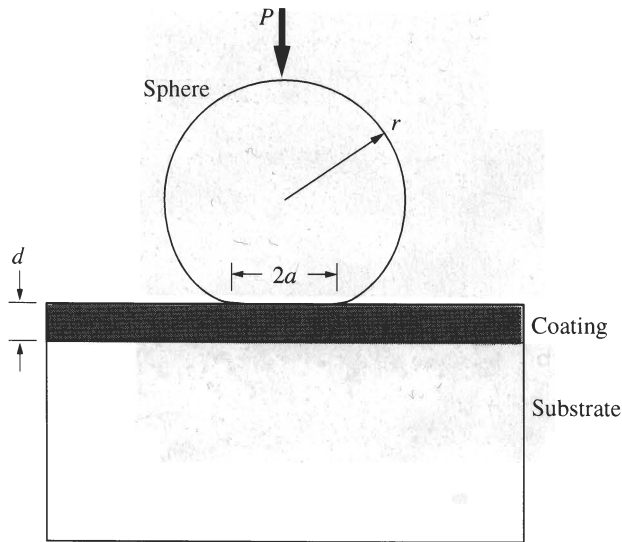


Fig. 2. Schematic of Hertzian test. Sphere of radius r on coating thickness d produces contact of radius a at load P . Scaling of a and d with r preserves geometrical similarity in contact field.

Indentation stress–strain curves were first obtained for each composite coating/layer system, as well as for free-standing coatings and substrates. Measurements of the contact radius a at each prescribed sphere radius r and load P were made at the impressions, to enable evaluations of indentation stress ($p_0 = P/\pi a^2$) as a function of indentation strain (a/r). For the coating surfaces, a precursor gold film greatly assisted delineation of the actual contact area, especially at lower contact pressures [7].

Bonded-interface specimens were then prepared for profile views of damage zones [8]. This entailed cutting sections of the coating/substrate composite with a diamond wheel, polishing the cut sections, and tightly screwing together the two mating half-blocks through carefully aligned holes in the metal substrates. This last step using screws was adopted because the conventional adhesive [8,9] did not provide a sufficiently strong bond, especially with the metal substrate. Single-cycle indentations were made with the spherical indenters along the trace of the bonded-interface on the top coating surface. The indented specimens were then separated, cleaned and gold coated, and viewed optically in Nomarski interference contrast.

Some supplementary Vickers indentation tests were made to measure indentation hardness $H = 2P/d^2$ (d the impression diagonal) in both bulk coating and substrate materials.

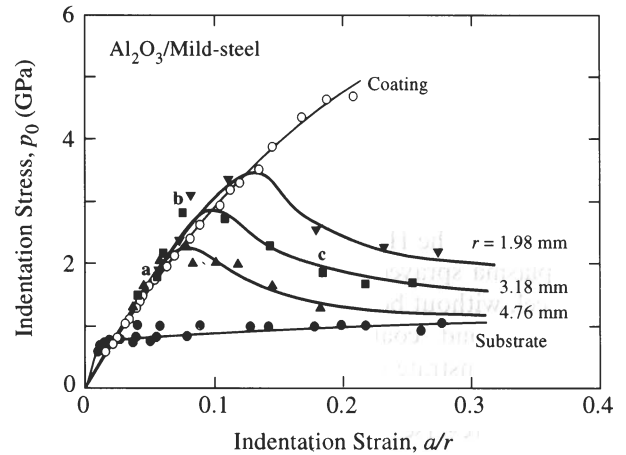


Fig. 3. Indentation stress–strain curve for alumina/steel, coating thickness $d = 500 \mu\text{m}$. Data for free-standing coating and substrate plotted for sphere radius $r = 1.98$ to 12.7 mm (not distinguished). Data for coating/substrate composites plotted separately for designated values of sphere radius: $r = 1.98$ mm ($d/r = 0.25$), $r = 3.18$ mm ($d/r = 0.16$), $r = 4.76$ mm ($d/r = 0.11$). Solid curves are empirical data fits. (Points a, b, c on coating/substrate curve correspond to load sequence in Fig. 5.)

3. Results

3.1. Indentation stress–strain curves

Indentation stress–strain curves, $p_0(a/r)$, for the two coating/substrate systems are plotted in Fig. 3, for alumina/steel, and Fig. 4, for zirconia/bond-coat/superalloy, for specified values of indenter radius. In these figures, results for free-standing coatings and substrates are included as limiting states. Individual data points represent single indentations, and the solid lines represent corresponding empirical fits.

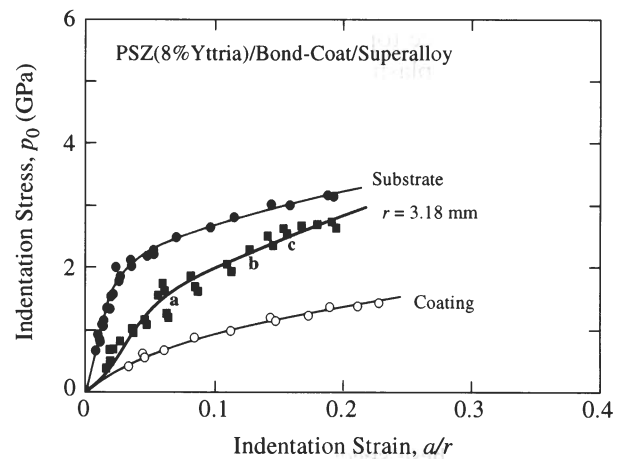


Fig. 4. Indentation stress–strain curve for zirconia/bond-coat/superalloy, coating thickness $d = 300 \mu\text{m}$. Data for free-standing coating and substrate plotted for values of $r = 1.98$ to 12.7 mm (not distinguished). Data for coating/substrate composites plotted for single value of $r = 3.18$ mm ($d/r = 0.094$). Solid curves are empirical data fits. (Points a, b, c on coating/substrate curve correspond to load sequence in Fig. 6.)

For the free-standing coatings and substrates, we observe monotonically increasing stress–strain curves in Figs. 3 and 4. Initially, the responses are near-linear according to the Hertz contact relation for homogenous elastic solids [18,19]:

$$p_0 = (3E/4\pi k)a/r$$

where E is Young's modulus, $k = (9/16)[(1 \pm \nu^2) + (1 \pm \nu^2)E/E']$ is a dimensionless coefficient, with ν Poisson's ratio and the prime notation denoting the indenter material. Ultimately, however, the free-standing curves depart from linearity at higher strains, indicating the onset of "yield" in the material, but nevertheless still according to a universal $p_0(a/r)$ function, independent of r [19,20].

For the composite coating/substrate systems in Figs. 3 and 4, the stress–strain response varies within the limits of the coating and substrate curves, according to the relative hardnesses of coating and substrate (Table 1).

3.1.1. Alumina/steel (Fig. 3)

The coating is considerably harder than the substrate. Data sets for the composite coating/substrate are plotted for three indenters, radius $r = 1.98, 3.18$ and 4.76 mm. With increasing contact load, each such data set initially follows close to the free-standing coating curve, but then passes through a maximum, and finally approaches the substrate curve. The implication is that the load is initially supported elastically by the coating, and ultimately plastically by the substrate. The maximum shifts progressively to lower stresses and strains with increasing r . The $p_0(a/r)$ curve is no longer a universal function, but now depends on the relative coating thickness, d/r .

3.1.2. Zirconia/bond-coat/superalloy (Fig. 4)

The substrate is harder than the coating. Data for the coating/substrate system are plotted for a single sphere radius $r = 3.18$ mm. In this case the data deviate from the coating curve at low strains toward the substrate curve at high strains.

Hence there are elements of similarity and difference in the stress–strain curves for the two coating/substrate systems. In both, the properties of the coating govern at low strains, those of the substrate at high strains. On the contrary, whereas in the alumina/steel system the low–high strain states are separated by a maximum, in the zirconia-bond-coat/superalloy system the curve is monotonic. Accordingly, the mechanical role of the coating in relation to the substrate may be viewed as hardening in alumina/steel, and softening in zirconia-bond-coat/superalloy.

Vickers hardness values for each coating and substrate material are included in Table 1.

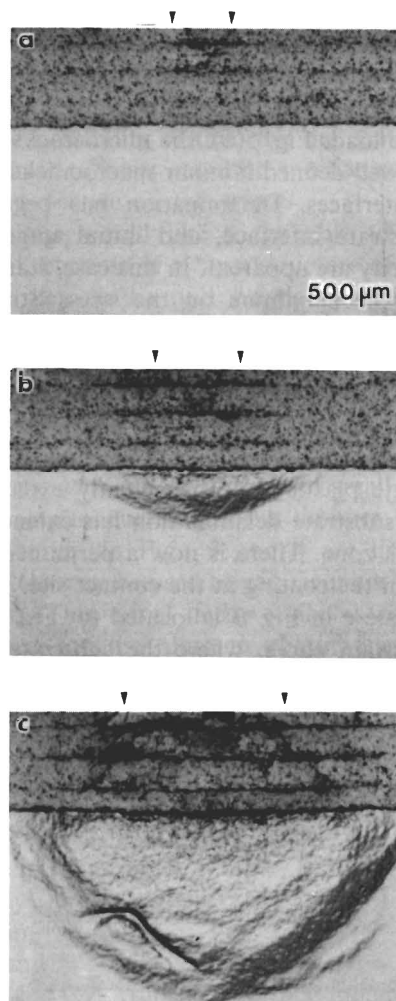


Fig. 5. Optical micrographs of section from bonded-interface specimen of alumina/steel, at peak loads $P =$ (a) 150 N, (b) 500 N and (c) 1500 N. Contact diameters indicated by arrows. Note fracture damage in coating, notably along intralayer planes and at coating/substrate interface (delamination), and large-scale plasticity in substrate. Corresponding indentation stresses and strains indicated as a, b, c in Fig. 3. Nomarski illumination. (Dark marking at lower left in substrate plastic zone in c is artifact from spurious contact between bonded-interface metal halves.)

3.2. Contact damage characterization

Micrographs of subsurface Hertzian contact damage on bonded-interface sections are presented for alumina/steel in Fig. 5 and zirconia/bond-coat/superalloy in Fig. 6, for a single sphere radius $r = 3.18$ mm. In the two material systems the micrographs are shown at low, intermediate, and high contact deformations, designated by the points a, b and c on the appropriate stress–strain curves in Figs. 3 and 4.

3.2.1. Alumina/steel system

Fig. 5 shows the evolution of damage with expanding contact. At low load, Fig. 5(a), initial stages of damage appear at the intra-coating interfaces, in the form of localized microcracking. At the same time, the corre-

sponding state **a** in Fig. 3 remains on the rising portion of the stress–strain curve, indicating that the bulk of the load is supported elastically by the coating. At intermediate load, Fig. 5(b), the microcracks have coalesced into well-defined laminar macrocracks along the defective interfaces. Delamination has begun at the coating/substrate interface, and initial stages of substrate plasticity are apparent. In this case, state **b** in Fig. 3 lies near the maximum on the stress–strain curve, signalling the beginnings of yield. At high load, Fig. 5(c), the intra-coating macrocracks have continued to develop, and to link up to form an inverted cap-like failure surface which traverses the interlayers, as if the indenter has partially “punched” through the coating. The substrate plastic zone has greatly expanded, and the coating/substrate delamination has extended to the edges of this zone. There is now a permanent residual depression in the coating at the contact site. The corresponding state **c** in Fig. 3 is located toward the tail of the stress–strain curve, where the substrate deformation dominates the response.

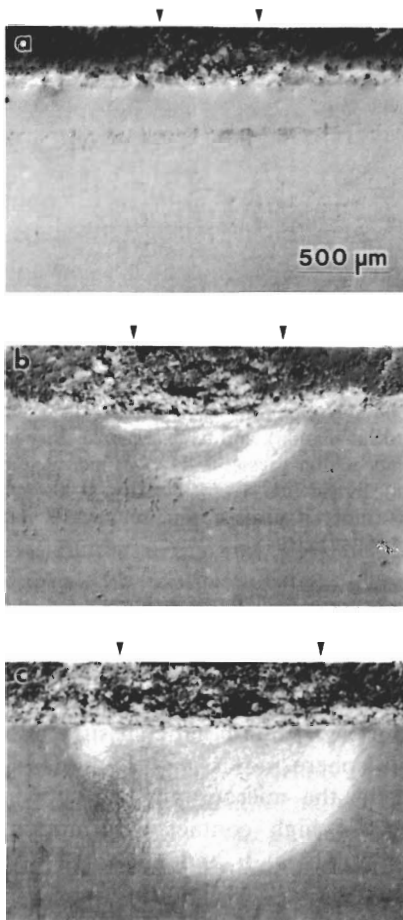


Fig. 6. Optical micrographs of section from bonded-interface specimen of zirconia/bond-coat/superalloy, at peak loads $P =$ (a) 400 N, (b) 1500 N and (c) 2500 N. Contact diameters indicated by arrows. Note fracture damage within coating but not at bond-coat interfaces, plasticity in substrate. Corresponding indentation stresses and strains indicated as **a**, **b**, **c** in Fig. 4. Nomarski illumination.

3.2.2. Zirconia/bond-coat/superalloy system

Fig. 6 shows a similar evolutionary sequence. Again, at small load, Fig. 6(a), limited initial microcracking is evident, near but not at the coating/bond-coat interface. There is no indication of any substrate deformation at this stage. The corresponding state **a** on the stress–strain curve in Fig. 4 lies intermediate between the two limiting curves, suggesting that the elastic deformation at this point is distributed almost equally within coating and substrate. At intermediate load, Fig. 6(b), macrocracks have developed in the coating, and the substrate has deformed plastically. Note, however, that there is no delamination at the bond coat interfaces, suggesting relatively strong bonding with coating and substrate. State **b** in Fig. 4 has now advanced well up the stress–strain curve, toward the substrate-dominated region. At high load, Fig. 6(c), microfracture damage in the coating and plasticity in the substrate are extensively developed, but still without bond-coat delamination. There is a substantial residual depression in the coating layer, reflecting the pervasive influence of the substrate deformation. Point **c** now lies in the stress–strain tail of Fig. 4.

Thus coating failure in both systems occurs by microcrack coalescence into laminar macrocracks within the concentrated stress field. The damage accumulation becomes most pronounced once substrate plastic deformation occurs. In the alumina/steel system, defect layers enhance macrocrack formation and the absence of a bond coat enhances interface delamination. Note, however, that even in the zirconia/bond-coat/superalloy fracture damage still accumulates effectively. In the fully developed states, Figs. 5(c) and 6(c), the coating macrocracks extend only slightly beyond the contact diameter, indicating some form of transverse coating rupture at the edges of the contact [21]. There is also considerable residual deflection in the heavily deformed coatings. The scale of damage in both still-intact coatings is reflective of unusually high damage-tolerant structures.

4. Discussion

Hertzian contact offers a uniquely simple, economical, and controlled approach to the characterization of fracture/deformation properties in ceramic/metal coating structures. It is particularly useful for identifying weak points in the structures, and enables the evaluation of important elastic–plastic variables in the mechanical response. The test itself is not promoted as an idealized simulation of loading configurations that might be experienced in many important practical applications, as for instance in the thermal cycling of thermal barrier coatings. Its main potential strength in the context of design would appear to be as a route to

materials evaluation, without the complexity of rig testing. Nevertheless, the contact test does retain an obvious relevance to bearing applications, particulate impacts, erosion, etc. Extension of the test to fatigue testing, by repeated loading on the indenting sphere, is a trivial matter [7,22,23].

Consider first the qualitative aspects of the test data. The micrographs in Figs. 5 and 6 reveal the development of extensive damage with increasing contact load. The evolution of macroscopic laminar cracks from incipient microcrack sources on places of weakness is evident in the coatings. However, the substrate and bond coat also play critical roles in the macroscopic damage. The substrate absorbs energy from the loading in the form of plastic deformation, particularly in the relatively soft steel in Fig. 5. Noting the intrinsic irreversibility in these fracture and deformation processes, especially in the plasticity, there is the expectation of considerable coating/substrate mismatch in the stress and strain fields. This mismatch accounts for the large residual openings in the macroscopic cracks. Much of the mismatch may be expected to occur on indenter unloading, as the compression stresses from the elastic component of the contact field are released [24] and the coating recovers relative to the substrate. The presence of the bond coat in the zirconia system of Fig. 6 inhibits delamination at the interface with the substrate, but is unable to prevent cracks from opening up within the coating. Substantial residual depression is observed in the coating in Figs. 5 and 6, indicating inordinately large “plate flexure” over the contact diameter, accounting in part for the transverse fractures [21]. The fact that the coating systems can sustain such massive damage and still remain intact attests to their impressive damage tolerance, although the capacity of these coatings to sustain still higher loads without total failure is open to question.

The indentation stress–strain curves in Figs. 3 and 4 provide a useful graphical indication of the extent of damage accumulation, in terms of the pronounced deviations from ideal linear elastic responses. As is clear from Fig. 3, the stress–strain curve depends on the coating thickness. More specifically, noting from Fig. 2 that scaling both contact radius a and coating thickness d with the sphere radius r effectively preserves the geometrical similarity of the contact field [20], we can argue that the function $p_0(a/r)$ for any given layer system must be uniquely determined by d/r . Further, noting that the depth of damage scales with a in Figs. 5 and 6, the shape of the $p_0(a/r)$ function allows us to distinguish regions of coating- or substrate-controlled damage: at small a/d , the damage zone is contained largely within the coating, and the role of the substrate is minimal; at large a/d , the damage zone extends well beyond the confines of the coating, and the substrate takes up the bulk of the support. For alumina/steel

(Fig. 3), the coating effectively hardens the underlayer. Conversely, for zirconia/bond-coat/superalloy (Fig. 4), the coating softens the underlayer. These considerations suggest the possibility of tailoring the coating material and thickness to meet requisite mechanical properties for any prospective contact event.

Ideally, one would like to be able to predict the mechanical response of a layer structure of given thickness from key elastic and plastic parameters of the constituent coating and substrate materials. The indentation stress–strain curves for the free-standing materials in Figs. 3 and 4 lend themselves to quantitative evaluations of these key parameters:

(i) *Elastic modulus.* In the domain of small loads where the stress–strain curves for the limiting coating and substrate curves in Figs. 3 and 4 are linear proportional, Eq.(1) may be used to gain estimates of Young’s modulus E . This initial linear region is comparatively well defined for the alumina coating in Fig. 3 and superalloy substrate in Fig. 4, up to $p_0 \approx 1.5$ GPa in each case; the corresponding uncertainty in slope measurement in this domain is estimated at less than $\pm 5\%$. On the contrary, for the steel substrate in Fig. 3 and zirconia coating in Fig. 4 nonlinearity is apparent at much lower loads, and only the first two or three data points are included in the evaluations; in these cases the uncertainty in slope is probably in excess of $\pm 20\%$. The ensuing estimates of E from Eq. (1) with uncertainty bounds listed in Table 1 are made using $E' = 614$ GPa and $\nu' = 0.22$ (tungsten carbide indenter) and $\nu = 0.25$ (specimen materials). The estimates obtained may be compared with the following literature values for fully dense bulk materials (with typical spread ± 20 GPa): 380 GPa for alumina; 200 GPa for soft steel; 210 GPa for zirconia; 200 GPa for superalloy. Thus, whereas the results for the substrate metals are consistent with the literature values within the limits of uncertainty, those for the ceramic coatings are much reduced, to 20% in the case of alumina and 14% in zirconia. Such large discrepancies are not atypical of plasma-sprayed ceramics with porosities as high as those listed in Table 1 [4].

(ii) *Yield stress.* The coating and substrate stress–strain curves in Figs. 3 and 4 show distinctive nonlinearities, implying some yield process. This is true not only for the metal substrates but also for the ceramic coatings, particularly zirconia in Fig. 4. The onset of plasticity is predicted to occur when the maximum shear stress $0.47p_0$ in the Hertzian field (located at a depth $0.5a$ below the contact axis) reaches one half the uniaxial yield stress Y , corresponding to a point of deviation $p_0 \approx 1.1Y$ on the stress–strain curve [20,25]. This point of first deviation is difficult to determine directly from the stress–strain curves in Figs. 3 and 4, especially with

the limited number of data points in the small strain regions. Accordingly, we may instead obtain first estimates of Y from the hardness values in Table 1 using the relation $Y = H/C$, where $C \approx 2.8$ is a plastic “constraint factor” [20]. The appropriately computed values $p_0 = 1.1Y = 2.1$ GPa for alumina, 0.46 GPa for steel, 0.70 GPa for zirconia, and 1.7 GPa for superalloy, would appear to provide reasonable elastic-limit bounds for the free-standing coating and substrate curves in Figs. 3 and 4.

Such parametric calibrations open the way to *a priori* evaluations of the stress–strain responses for the composite coating/substrate systems, using for example finite element modelling [21,26]. Modelling of this kind is currently under way, in an effort to account for the trends in Figs. 3 and 4, and to determine the intralayer and interlayer stress distributions responsible for the fracture and deformation patterns. Such modelling may also help to understand several other design-related issues. How does the damage accumulate during the loading cycle? When does fracture form in the coating, e.g. during loading or unloading? Does this fracture seriously impair the capacity of the coating to continue sustaining the contact load? What is the role of substrate plasticity in the coating failure? Is “yield” in the coating properly described by a conventional shear-driven process, or by some pressure-driven compaction of the open structure? What is the effect of elastic–plastic mismatch on the stress field, and what coating thicknesses best minimize the more dangerous components of this field? How do the contact observations relate to the stress states experienced in more traditional thermal cycling tests [27], and can we use observations from the former to make failure predictions in the latter?

An important implication deriving from this study concerns the role of microstructure in the damage accumulation. Mention has been made of the high density of weak internal interfaces and porosity that characterize plasma sprayed coatings, and allusion made as to how these defects may actually benefit damage tolerance. Contact testing presents itself as a particularly attractive diagnostic means for probing sources of weakness in the coatings, and thereby for optimizing plasma spray variables for maximum damage tolerance. Accordingly, there is a need for more detailed microstructural characterization of coating structures, before, during and after the onset of damage. In particular, the manner in which such microstructural variables as grain boundary toughness, splat size and shape, porosity, residual stresses, etc. govern the coating failure may be usefully explored using the Hertzian test.

5. Conclusions

(i) Hertzian contact testing was used to probe sources of incipient microstructural failure in alumina and zirconia plasma sprayed ceramic coatings on steel and superalloy substrates, respectively.

(ii) Indentation stress–strain curves were used to quantify the relative role of the coating and substrate in the net deformation response. These curves show a transition from a coating-controlled response at low strains to a substrate-controlled response at high strains, with an intervening maximum for the alumina/steel system.

(iii) Damage processes within the coating and substrate were studied using “bonded-interface” specimens. Coating degradation occurred by laminar cracking at the interface with the substrate (delamination) and within the coating itself. Plastic deformation, primarily in the metal substrate but also in the coating, contributed to the crack driving force.

(iv) Evaluations of elastic moduli and yield stresses were made from the indentation stress–strain data.

Acknowledgements

This work was supported by the U.S. Air Force Office of Scientific Research and the National Science Foundation. Special financial support for A. Pajares from the Ministerio de Educación y Ciencia (DGI-CYT), Spain, is acknowledged. Thanks are due to G. Bancke for assistance in preparing the coatings, and to E.R. Fuller for the computer evaluations of porosities in the coating materials.

References

- [1] H. Herman, *Sci. Am.*, 256 (1988) 113–188.
- [2] H. Herman, *Mater. Res. Soc. Bull.*, 13 (1988) 60–67.
- [3] H. Herman, C.C. Berndt, H. Wang, in J.B. Wachtman and R.A. Haber, (eds.), *Ceramic Films and Coatings*, Noyes Publications, Park Ridge, NJ, 1993. pp. 131–188.
- [4] L. Pawlowski, *The Science and Engineering of Thermal Spray Coatings*, Wiley, New York, 1995.
- [5] J.C. Knight, T.F. Page and I.M. Hutchings, *Thin Solid Films*, 177 (1989) 117–132.
- [6] A.H. Bartlett and R.D. Maschio, *J. Am. Ceram. Soc.*, 78 (1995) 1018–1024.
- [7] F. Guiberteau, N.P. Padture, H. Cai and B.R. Lawn, *Philos. Mag.*, A68 (1993) 1003–1016.
- [8] F. Guiberteau, N.P. Padture and B.R. Lawn, *J. Am. Ceram. Soc.*, 77 (1994) 1825–1831.
- [9] H. Cai, M.A. Stevens Kalceff and B.R. Lawn, *J. Mater. Res.*, 9 (1994) 762–770.
- [10] N.P. Padture and B.R. Lawn, *J. Am. Ceram. Soc.*, 77 (1994) 2518–2522.
- [11] H.H.K. Xu, L. Wei, N.P. Padture, B.R. Lawn and R.L. Yeckley, *J. Mater. Sci.*, 30 (1995) 869–878.
- [12] A. Pajares, F. Guiberteau, B.R. Lawn and S. Lathabai, *J. Am. Ceram. Soc.*, 78 (1995) 1083–1086.

- [13] P.L. Swanson, C.J. Fairbanks, B.R. Lawn, Y.-W. Mai and B.J. Hockey, *J. Am. Ceram. Soc.*, 70 (1987) 279–289.
- [14] B.R. Lawn, *Fracture of Brittle Solids*, Cambridge University Press, Cambridge, 1993.
- [15] B.R. Lawn, N.P. Padture, H. Cai and F. Guiberteau, *Science*, 263 (1994) 1114–1116.
- [16] L. An, H.M. Chan, N.P. Padture and B.R. Lawn, *J. Mater. Res.*, 11 (1996) 204–210.
- [17] S. Wuttiphon, B.R. Lawn and N.P. Padture, *J. Am. Ceram. Soc.*, 79 (1996) 634–640.
- [18] S. Timoshenko and J.N. Goodier, *Theory of Elasticity*, McGraw-Hill, New York, 1951.
- [19] M.V. Swain and B.R. Lawn, *Phys. Stat. Solidi*, 35 (1969) 909–923.
- [20] D. Tabor, *Hardness of Metals*, Clarendon, Oxford, 1951.
- [21] P. Montmitonnet, M.L. Edinger and E. Felder, *ASME J. Tribol.*, 115 (1993) 15–19.
- [22] H. Cai, M.A.S. Kalceff, B.M. Hooks, B.R. Lawn and K. Chyung, *J. Mater. Res.*, 9 (1994) 2654–2661.
- [23] N.P. Padture and B.R. Lawn, *J. Am. Ceram. Soc.*, 78 (1995) 1431–1438.
- [24] B.R. Lawn, A.G. Evans and D.B. Marshall, *J. Am. Ceram. Soc.*, 63 (1980) 574–581.
- [25] R.M. Davies, *Proc. R. Soc. London*, A197 (1949) 416–432.
- [26] K. Komvopolous, *ASME J. Tribol.*, 111 (1989) 430–439.
- [27] R.A. Miller, *Surf. Coat. Technol.*, 30 (1987) 1–11.